ROYAL SOCIETY
OF CHEMISTRY

PAPER

Check for updates

Impact of solution temperature-dependent aggregation on the solid-state packing and electronic properties of polymers for organic photovoltaics†

Ajith Ashokan, ‡[a] Tonghui Wang, ‡[a] Mahesh Kumar Ravva [b] and Jean-Luc Brédas *[a]

The performance of a bulk-heterojunction organic solar cell critically depends on the morphology of the active layer. The solution temperature-dependent aggregation characteristics of a series of polymer donors have been recently exploited as an effective protocol for morphology control in high-efficiency devices. Here, we use an approach combining molecular dynamics simulations and long-range corrected density functional theory calculations to investigate the impact of solution temperature-dependent aggregation on the polymer solid-state packing and electronic properties. We consider two representative polymer systems: (i) PffBT4T-2OD (poly[(5,6-difluoro-2,1,3-benzothiadiazol-4,7-diyl)-*alt*-(3,3′′′-di(2-octyldodecyl)-2,2′;5′,2′′;5′′,2′′′-quaterthiophen-5,5′′′-diyl)]), and (ii) PBT4T-2OD (poly[(2,1,3-benzothiadiazole-4,7-diyl)-*alt*-(3,3′′′-di(2-octyldodecyl)-2.2′;5′,2′′;5′′,2′′′-quarterthiophen-5,5′′′-diyl)]), where the fluorine atoms on the benzothiadiazole moieties of PffBT4T-2OD are replaced with hydrogen atoms. We find that both temperature-dependent aggregation and the presence of fluorine atoms are important in determining the nature of the solid-state packing and the electronic properties in the polymer phases. Our results are consistent with the experimental data that show that PffBT4T-2OD aggregates at lower temperatures and leads to higher OPV efficiency.

1. Introduction

In organic solar cells, the bulk heterojunction (BHJ) nature of the active layer is now well established as a key element to realize higher power conversion efficiencies (PCEs). The prospect of large-scale roll-to-roll processing of polymer materials on flexible substrates at low cost is giving organic photovoltaics (OPV) technology a promising edge among renewable energy technologies. With the development of efficient polymer donors and non-fullerene acceptors, PCEs as high as 14.2% in single-junction devices and 17.3% in tandem cells have recently been achieved.[1,2]

Many investigations have underlined the central role played by the active-layer morphology in promoting high PCE values.[3–20]

Active layers with a binary architecture often display a three-phase arrangement: a polymer donor-rich phase, an acceptor-rich phase, and a mixed donor–acceptor amorphous phase.[3–8] Generally, OPV devices with higher PCE values possess donor and acceptor domains with good crystallinity and reasonably small sizes (typically 20–40 nm). Also, resonant soft X-ray scattering and atomic force microscopy experiments have revealed the importance of domain purity in improving device performance.[19–21] Overall, improving the morphology characteristics of the active layer remains an important step in obtaining higher device efficiencies.

Significant efforts have been devoted to try and control the active layer morphology *via* techniques including thermal or solvent annealing,[22–26] chemical substitution of the polymer donor and/or acceptor,[11–13,16–19,24–27] the use of solvent additives,[20,25–27] and/or varying the donor–acceptor ratios in the active layer. Recently, Yan and co-workers demonstrated the successful exploitation of the solution temperature-dependent aggregation properties of a series of polymers in achieving efficient morphology control.[17–19] Temperature-dependent aggregation can be used to direct the polymers to form domains with optimal 20–40 nm sizes, which is conducive to high device performance.

[a] *School of Chemistry and Biochemistry & Center for Organic Photonics and Electronics (COPE), Georgia Institute of Technology, Atlanta, Georgia 30332-0400, USA. E-mail: jean-luc.bredas@chemistry.gatech.edu*

[b] *Physical Science and Engineering Division, KAUST Solar Center (KSC), King Abdullah University of Science and Technology (KAUST), Thuwal 23955-6900, Kingdom of Saudi Arabia*

† Electronic supplementary information (ESI) available. See DOI: 10.1039/c8tc05378b

‡ These authors contributed equally to this work.

We note that most of the polymers displaying temperature-dependent aggregation properties have fluorine atoms along the polymer backbone.[17–19] Interestingly, when removing the fluorine atoms from the backbones, the TDA properties tend to disappear and, in this context, lower device efficiencies are observed.[17–19] In some instances, the domain sizes for non-fluorinated polymers in the active layer were found to be very large (up to ~100 nm). Also, up to four-fold differences in device efficiencies were observed between polymers with and without TDA properties. For example, in the cases of blends of PBT4T-2OD (poly[(2,1,3-benzothiadiazole-4,7-diyl)-*alt*-(3,3′′′-di(2-octyldodecyl)-2.2′;5′,2′′;5′′,2′′′-quarterthiophen-5,5′′′-diyl)]) and PffBT4T-2OD (poly[[(5,6-difluoro-2,1,3-benzothiadiazol-4,7-diyl)-*alt*-(3,3′′′-di(2-octyldodecyl)-2,2′;5′,2′′;5′′,2′′′-quaterthiophen-5,5′′′-diyl)]]) with PC$_{71}$BM, the device efficiencies were measured to be 2.6% and 10.5%, respectively.[17,19] Thus, in order to gain a better understanding of the relationship between the morphology of the active layer and efficiency, it is useful to connect the TDA properties of the polymer donors with the fluorination of the backbone, as well as to consider the impact of the TDA properties on the inter-chain packing at the molecular level.

Here, we use a combination of molecular dynamics (MD) simulations and density functional theory (DFT) calculations to investigate the TDA properties of representative polymer donors and their impact on the formation of efficient morphologies and the nature of inter-chain packing. We chose the non-fluorinated polymer PBT4T-2OD and its difluorinated counterpart PffBT4T-2OD as model systems, see Fig. 1.

We start by discussing the results of MD simulations for the pure polymers in 1,2-dichlorobenzene solution at five different temperatures and characterize the differences in their extent of aggregation. We then rationalize these differences by analyzing the planarity of the PBT4T-2OD and PffBT4T-2OD backbones. Finally, we evaluate the impact of the temperature-dependent aggregation properties on the solid-state packing and electronic properties of the two polymers.

2. Methodology

2.1. Molecular dynamics simulations

The MD simulations were performed[28] with the LAMMPS package based on the Optimized Potential for Liquid Simulations - All Atom (OPLS-AA) force field.[29–32] The OPLS-AA force field was parameterized with bond lengths, bond angles, torsion angles, and atomic charges coming from PBT4T-2OD and PffBT4T-2OD oligomers optimized at the density functional theory (DFT) ωB97XD/6-31G(d,p) level. The torsion potentials for specific dihedral angles were calculated on oligomers of increasing size until convergence was achieved. The atomic partial charges were evaluated using the restricted electrostatic potential fitting scheme (RESP) at the ωB97XD/cc-PVTZ level of theory. We obtained very good fitting of the force-field with the updated parameters, as described in our previous work.[10] Here, all the DFT calculations were performed with the Gaussian 09-D01 package[33] and the RESP calculations were carried out with Red software.[34]

The initial models for the MD simulations were built by constructing polymer stacks (consisting of six polymer chains perfectly packed on top of each other) for both PBT4T-2OD and PffBT4T-2OD (see ESI,† Fig. S1 and S2); each polymer chain is 6 repeat-units long. The simulation boxes consisted of 152 448 atoms in total, including 12 226 1,2-dichlorobenzene (o-DCB) molecules. Here, the MD simulations were performed for both polymers at 100 °C (for 50 ns), 80 °C (for 80 ns), 60 °C (for 120 ns), 40 °C (for 200 ns) and 25 °C (for 200 ns); in the latter case, the time scale of 200 ns represents the limit of our MD simulations while at 100 °C, 80 °C, and 60 °C, the stacks nearly disaggregate into individual chains after 50 ns, 80 ns, and 120 ns, respectively.

We note that we tried initially to follow the experimental procedure and consider the aggregation rather than the disaggregation process. We randomly placed the polymer chains in the simulation box with the o-DCB molecules. The simulation box consisted of 20 PffBT4T-2OD polymer chains (each chain has 6 repeat units) and 7172 o-DCB molecules, which corresponds to a polymer concentration of 105.6 mg mL^{-1}. Although such a concentration is higher than the experimental value, chain aggregation occurs only at very long time scales, well beyond what is currently computationally feasible in terms of such MD simulations. We were thus forced to investigate rather the disaggregation process.

To examine more closely the planarity of individual chains, MD simulations were carried out on single chains. The simulation box for the PBT4T-2OD polymer consisted of 87 440 atoms (one chain of PBT4T-2OD and 7207 molecules of o-DCB) while that for the PffBT4T-2OD polymer contained 89 600 atoms (one chain of PffBT4T-2OD and 7387 molecules of o-DCB). Here, the simulations were carried out at 25 °C for 10 ns.
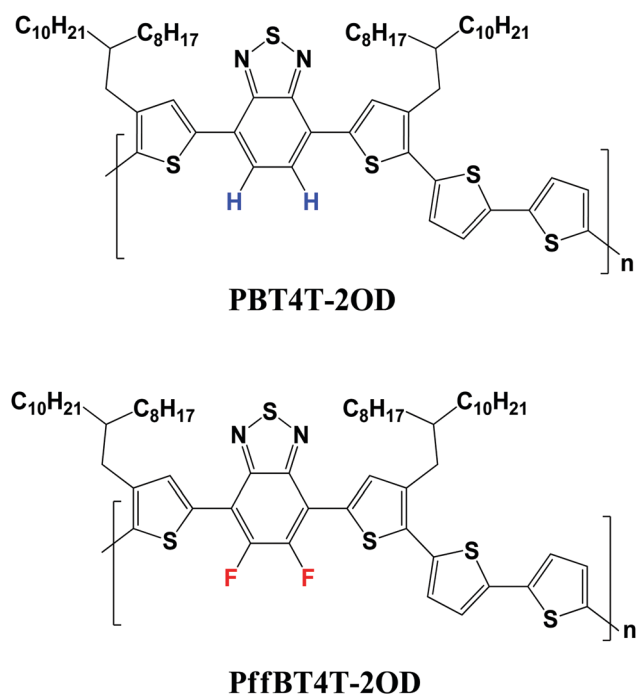

PBT4T-2OD

PffBT4T-2OD

Fig. 1   Illustration of the chemical structures of the PBT4T-2OD and PffBT4T-2OD polymers, highlighting their chemical difference.

2.2. Density functional theory calculations

All the DFT calculations were performed at the ωB97XD/6-31G(d,p) level of theory. In the framework of semi-classical Marcus theory, the electronic couplings (transfer integrals) among neighboring chains are a relevant figure of merit to describe at least qualitatively the charge-transport properties of the active layer.[35] The transfer integrals among sets of neighboring chains, *i.e.*, dimers extracted from MD simulation snapshots at different temperatures were calculated using a fragment orbital approach[36] combined with a basis set orthogonalization procedure. These calculations were performed with the Gaussian 09-D01 package.[33]

Another useful parameter in determining the strength of interaction among polymer chains is their binding energy. A higher binding energy between specific chain segments implies a higher probability of the presence of such interacting segments in the bulk phase of the active layer. In the evaluation of the binding energies, in order to prevent basis set superposition errors (BSSE), the counterpoise correction method proposed by Boys and Bernardi was applied.[37]

3. Results and discussion

3.1. Morphology of the polymers in solution

We first focus on the disaggregation of the polymer stacks as a function of time at five different temperatures representative of those used experimentally:

• For the PffBT4T-2OD and PBT4T-2OD stacks in solution at 100 °C and 80 °C disaggregation into individual chains takes place after 50 ns and 80 ns, respectively (see Fig. 2).

• At 60 °C, while the PBT4T-2OD stack disaggregates into isolated polymer chains after 120 ns, the PffBT4T-2OD stack separates into a smaller stack containing 3 interacting chains and into three separated chains; interestingly, the smaller 3-chain PffBT4T-2OD stack keeps long-range order.

• At 40 °C, the PBT4T-2OD stack starts to disaggregate along several sections after 200 ns; in contrast, the PffBT4T-2OD 6-chain stack begins to separate into two 4-chain and 2-chain stacks that clearly maintain the overall shape and long-range order compared to the PBT4T-2OD case.

• The simulations at 25 °C show trends similar to those at 40 °C in both cases; after 200 ns, the PffBT4T-2OD stack has separated into two smaller 3-chain stacks that keep their pattern and long-range order, while the PBT4T-2OD stack is seen to disaggregate along several sections.

The MD results are fully consistent with the experimental observations. Yan and co-workers indeed reported that PffBT4T-2OD chains aggregate when the solution is cooled down from 85 °C to room temperature, while PBT4T-2OD chains do not present any aggregation under the same conditions.[17,19] The ability of the PffBT4T-2OD chains to stack at 25 °C and 40 °C can be attributed to efficient chain packing in the aggregated state. This can be correlated with multiple observations that fluorination of the polymer backbone leads to more efficient π–π stacking in the solid state.[11–13,15–17] We note
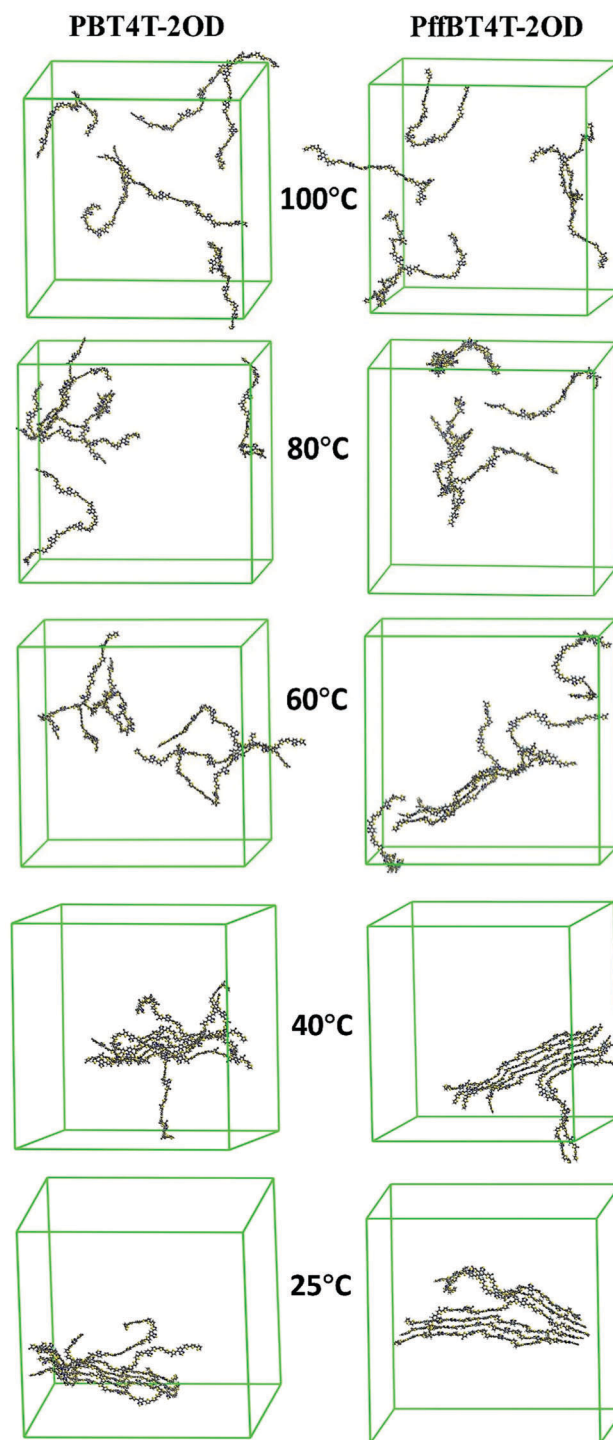

Fig. 2 Snapshots from the MD simulations showing the extent of disaggregation of the six polymer chains present in the simulation box. The snapshots on the left and right correspond to PBT4T-2OD and PffBT4T-2OD, respectively; they are taken from simulations at 100 °C (after 50 ns), 80 °C (after 80 ns), 60 °C (after 120 ns), 40 °C (after 200 ns) and 25 °C (after 200 ns).

that inter-chain H–F interactions could be a major driving force that leads to this effect in the PffBT4T-2OD polymer.[38] Since the PBT4T-2OD chains do not maintain any stacking configuration, be it at high or low solution temperatures, fluorination of the

polymer backbone is confirmed as a crucial factor directing chain aggregation at low temperature.

The simulations at 25 °C, 40 °C, and 60 °C reveal another major difference in the conformational behavior of the polymers. Unlike the PBT4T-2OD chains, the PffBT4T-2OD chains maintain long-range order throughout the simulations. Upon separation from the stack in solution, a PBT4T-2OD chain tends to bend, twist, and assume random conformations. Therefore, upon film casting, during the evaporation of the solvent molecules, the PBT4T-2OD chains are expected to remain in their disordered conformations; this, in turn, will lead to the formation of large, uncontrolled amorphous domains that can limit charge separation and thus result in lower device performance. On the contrary, the fact that the PffBT4T-2OD chains can maintain packing and long-range order in solution can translate into ordered domains in the solid state. Also, the low-temperature pre-aggregation of PffBT4T-2OD chains in solution allows the control of the eventual domain sizes in the solid state, *via* tuning of the solution temperature.

3.2. Distribution of dihedral angles along the polymer chains and assessment of co-planarity

To compare the relative planarity between the PBT4T-2OD and PffBT4T-2OD chains, we analyzed the distributions of dihedral angles present along the polymer backbones. We evaluated these distributions based on 2000 snapshots extracted from the final 10 nanoseconds of the MD simulations at each temperature.

We first discuss the dihedral-angle distributions for the polymer stacks in solution. Since the distributions turn out to be similar at the five temperatures, we describe here the 25 °C case while the distributions at higher temperatures (40 °C, 60 °C, 80 °C and 100 °C) are provided in the ESI.† Three dihedral angles, depicted in Fig. 3, have been chosen for this analysis. Dihedral **1** represents the torsion angle between the benzothiadiazole unit of the PBT4T-2OD polymer or di-fluoro-benzothiadiazole unit of the PffBT4T-2OD polymer and the thiophene unit on its right side. Dihedrals **2** and **3** represent the torsion angles between the two central and two external thiophenes of the quarterthiophene moieties.

A comparison of the dihedral distributions of both polymers reveals that, for dihedral angle **1**, there is a substantially higher relative frequency distribution of dihedral angles around $0° \pm 50°$ for PffBT4T-2OD as compared to PBT4T-2OD (see Fig. 4).
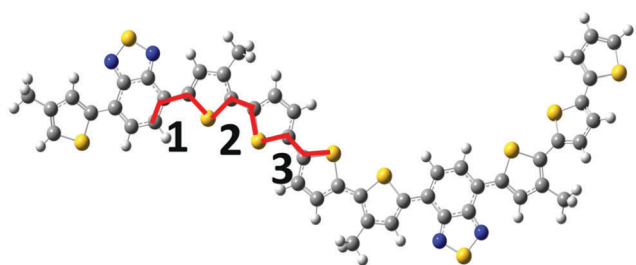

Fig. 3 Illustration of the three dihedrals considered to analyze the distribution of dihedral angles.

For dihedral angle **3**, PffBT4T-2OD has a strong distribution around $180° \pm 50°$ and a very limited distribution around $0° \pm 50°$, while PBT4T-2OD has a much narrower distribution around $+180°$ and a broad distribution around $0° \pm 50°$. For dihedral angle **2**, largely similar distributions are found for both polymers.

The results for dihedral angles **1** and **3** confirm that the PffBT4T-2OD polymer chains tend to be more planar as compared to the PBT4T-2OD polymer. As shown in Fig. S3–S6 (ESI†), these trends in dihedral-angle distributions are found to be similar at all the other temperatures. Since the side chains are the same on both polymers, their impact in determining the final stable conformations of both polymer chains is expected to be nearly identical.[10] With the only difference between the two polymers being the presence or absence of fluorine atoms in the polymer backbone, it is clear that the tendency of PffBT4T-2OD to remain more co-planar can be mainly ascribed to the backbone fluorination itself.

We also evaluated the dihedral-angle distributions of single polymer chains in *o*-DCB solution. Here, a single PBT4T-2OD/PffBT4T-2OD chain consisting of 6 repeat units was placed in solution; the simulations ran for 10 ns. Interestingly, we find similar trends for the distributions of all three dihedral angles, see Fig. 5. This result underlines that neither the solvent nor the effect of inter-chain interactions plays a significant role in determining the planarity of the PffBT4T-2OD chains. Thus, it is an intrinsic property of the PffBT4T-2OD chains to remain more co-planar in comparison to the PBT4T-2OD chains.

3.3. Binding energies and their effect on morphology

A way to quantify the strength of the inter-chain interactions is to consider the binding energies. We first evaluated the inter-chain binding energies for DFT-optimized PBT4T-2OD and PffBT4T-2OD dimers, where a dimer consists of two well-packed polymer chains with each chain containing two repeat units (see Table S1, ESI†). A difference of *ca.* 2 kcal mol^{-1} is calculated between the PffBT4T-2OD and PBT4T-2OD cases, which thus translates into *ca.* 1 kcal mol^{-1} per repeat unit.

We then estimated the binding energies between adjacent polymer chains extracted from the MD simulations of the polymer stacks in solution. Two chains in close proximity, consisting each of six repeat units, are taken as a dimer; thus overall, given six polymer chains, a maximum of five dimers can be present at any temperature. We note that at the higher temperatures of 80 °C and 100 °C, for which the polymer stacks disaggregate into individual chains, only the binding energies between chains that are somewhat close (<5 Å) are evaluated.

The binding energies between PffBT4T-2OD chains are found to be significantly larger than those between PBT4T-2OD chains (see Table 1). This is consistent with the fact that the simulations at lower temperatures, *e.g.*, at 25 °C and 40 °C, indicate that the PffBT4T-2OD chains remains better packed with longer-range order as compared to the PBT4T-2OD chains. Thus, adjacent PffBT4T-2OD chains have a longer interaction length. Considering the small difference in binding energy per repeat unit that we found between PffBT4T-2OD and PBT4T-2OD dimers, it is the
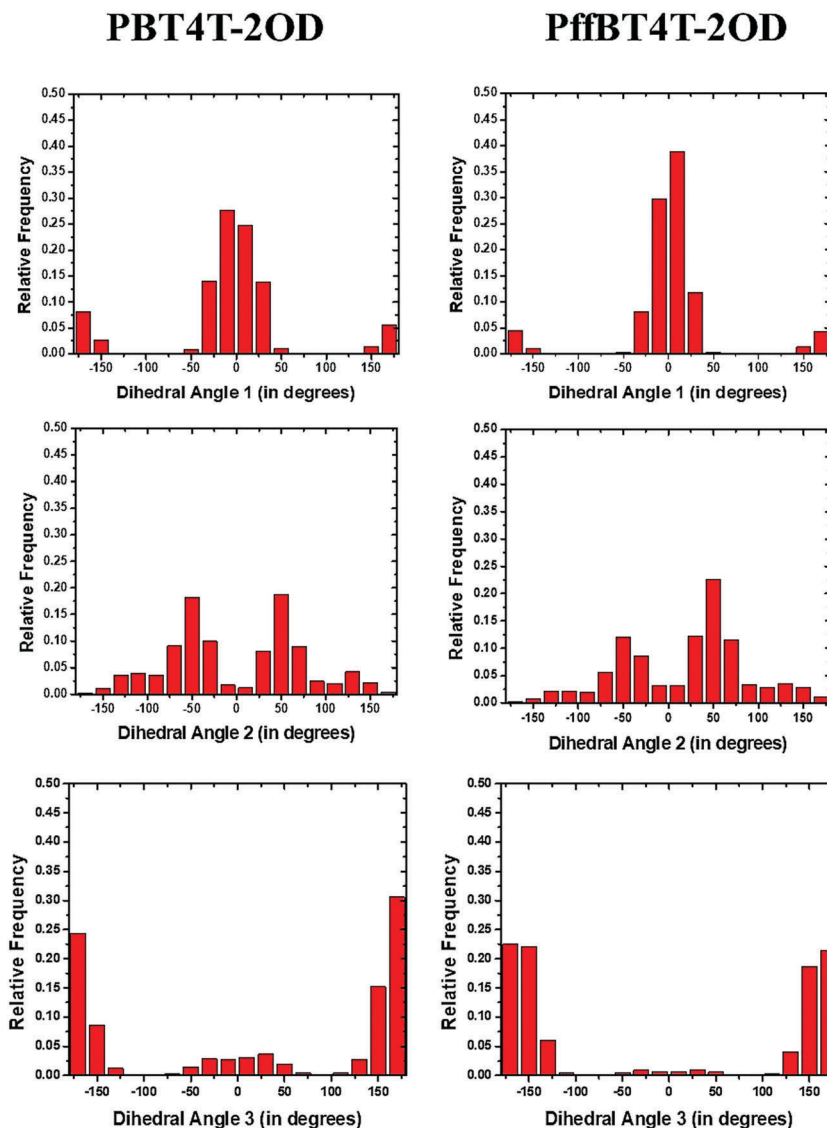
PBT4T-2OD

PffBT4T-2OD

Fig. 4   Distribution of dihedral angles along the PBT4T-2OD (left) and PffBT4T-2OD (right) chains after MD simulations of the respective polymer stacks in solution at 25 °C.

longer interaction length between the PffBT4T-2OD chains, and not the fluorination-induced increase in binding energy, that is mainly responsible for the significantly higher binding energies. Also, we note that the highest magnitude of binding energy for the PffBT4T-2OD chains is obtained at 25 °C, which correlates well with the largest extent of aggregation observed at that temperature.

3.4.   Electronic couplings

The electronic couplings (transfer integrals) are important parameters in the description of the charge-transport characteristics. As discussed above, the fact that the aggregation behavior and long-range packing order found in solution are expected to be maintained in the solid state, means that the electronic couplings for the chains in solution will be representative of the situation in the active layer.

Thus, we have evaluated the electronic couplings between adjacent PBT4T-2OD chains and PffBT4T-2OD chains extracted from the MD simulations of the polymer stacks in solution. The DFT calculations show that the HOMOs of both polymers delocalize across about two repeat units along the polymer backbone. For that reason, each chain (6 repeat-units long) was cut into 3 segments of two repeat units each; the HOMO–HOMO electronic couplings were then calculated between these segments (see Fig. S8 and S9, ESI†). We note that: (i) the electronic couplings between segments with inter-molecular distances larger than 5 Å are not evaluated since there is no effective wave-function overlap between such distant segments; and (ii) we only consider electronic couplings between HOMO levels since the polymers are hole transporters in the active layer.

At all solution temperatures (except 100 °C), the HOMO–HOMO couplings between PffBT4T-2OD segments are found to be consistently larger in comparison to the PBT4T-2OD case, see Fig. 6. We note that, at higher solution temperatures, the
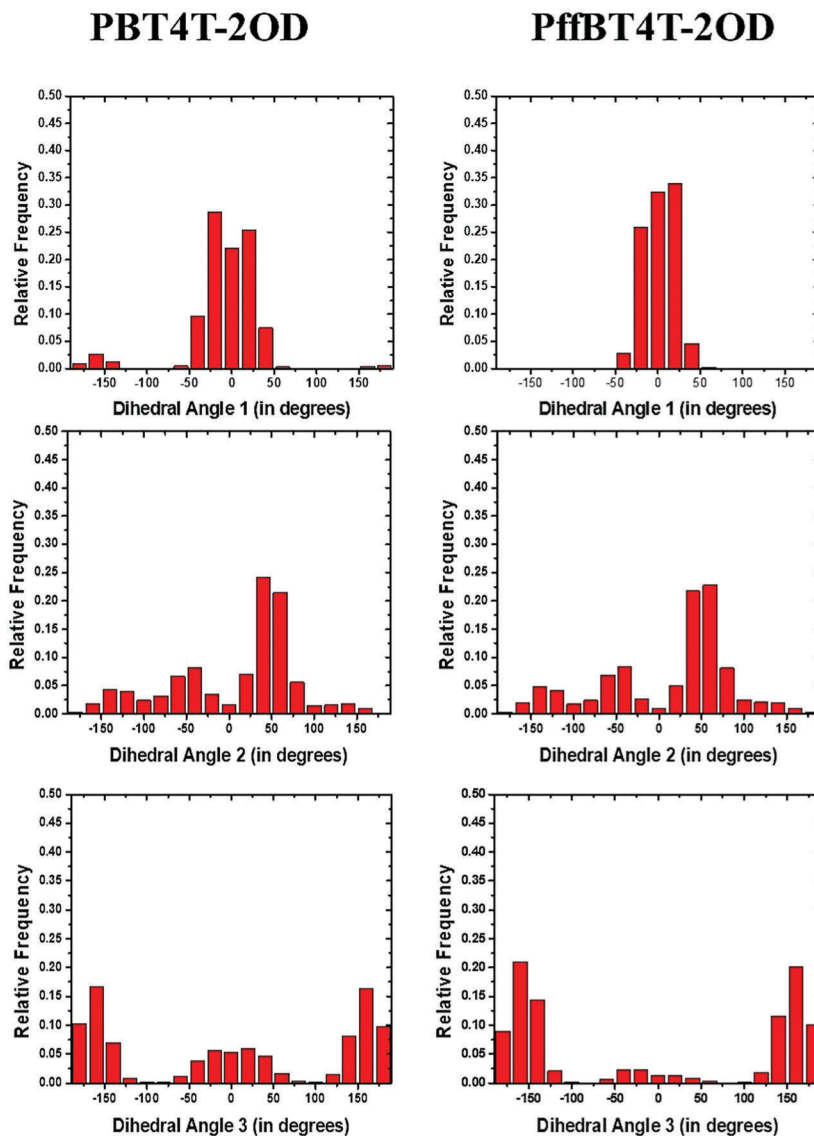
PBT4T-2OD   PffBT4T-2OD

Fig. 5 Distribution of dihedral angles along the PBT4T-2OD (left) and PffBT4T-2OD (right) chains after MD simulations of single polymer chains in *o*-DCB solution at 25 °C.

Table 1 Binding energies between two adjacent polymer chains, as calculated at the ωB97XD/6-31G** level of theory. A negative value indicates an attractive interaction

Polymer	Dimer	Binding energy (kcal mol^{-1})				
		25 °C	40 °C	60 °C	80 °C	100 °C
PBT4T-2OD	1	−99.7	−62.7	−25.4	−49.9	0
	2	−63.8	−49.0	0	0	0
	3	−50.6	−41.5	0	0	0
	4	−40.8	−23.1	—	—	—
	5	—	−18.2	—	—	—
PffBT4T-2OD	1	−120.5	−100.1	−87.9	−81.3	0
	2	−64.7	−89.3	0.0	−33.4	0
	3	−54.5	−87.9	0.0	0	0
	4	−2.2	−75.1	—	—	—
	5	—	−23.9	—	—	—

polymer segments separate and, consequently, there are very few interacting segments at 60 °C and 80 °C. At 100 °C, the polymer stacks are totally separated into individual chains and no interacting segments can be found within the threshold distance of 5 Å.

Overall, our investigations give useful insights that allow us to correlate the nature of the interactions in both polymers with the experimental results. The PffBT4T-2OD chains are observed experimentally to aggregate in solution at lower temperatures;[17,19] our MD simulations also show this pre-aggregation behavior as the PffBT4T-2OD stacks hold together at lower temperatures. The PffBT4T-2OD chains display better planarity, more efficient packing, and longer-range order in the stacks, leading to more efficient wave-function overlap between the chains; accordingly, we calculate higher electronic couplings among PffBT4T-2OD segments as compared to the PBT4T-2OD case.
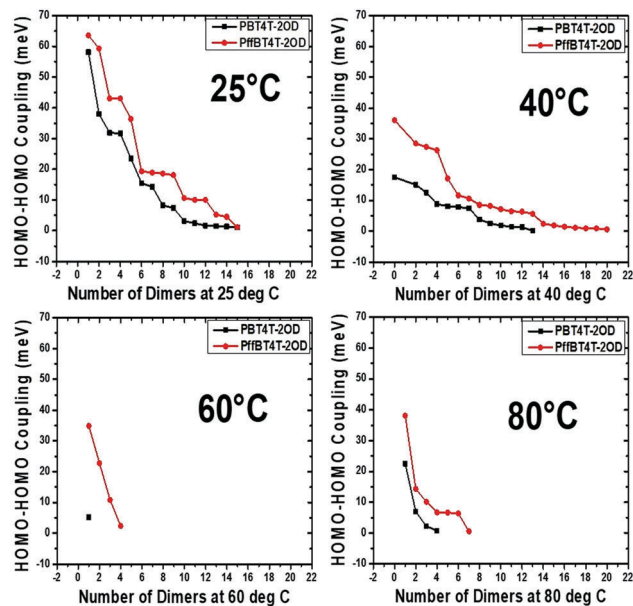
Fig. 6 Electronic couplings between segments of the PBT4T-2OD and PffBT4T-2OD chains at 25 °C, 40 °C, 60 °C and 80 °C.

4. Synopsis

We have investigated the effects of temperature-dependent aggregation on the solid-state packing and electronic properties of two representative polymers, PBT4T-2OD and PffBT4T-2OD, using a combination of MD simulations and long-range corrected DFT calculations.

Fluorination of the polymer backbone plays a key role in keeping the PffBT4T-2OD chains more co-planar than the PBT4T-2OD chains. The planarity of the polymer backbones in turn facilitates a longer interaction length between the polymer chains, as a result of which the PffBT4T-2OD chains remain well-packed in the stacks. These combined effects lead to easier pre-aggregation of the PffBT4T-2OD chains in solution.

Upon film formation, the solvent molecules evaporate; the well-aggregated nature of the PffBT4T-2OD chains is expected to be maintained in the solid state, which leads to adequate size morphologies in the active layer. This can contribute to efficient exciton diffusion and hole transport within the PffBT4T-2OD domains, and ultimately lead to higher device efficiency. The exploitation of the temperature-dependent aggregation properties thus represents an effective tool to control the morphology of the active layers.

Conflicts of interest

There are no conflicts to declare.

Acknowledgements

References

1 S. Li, L. Ye, W. Zhao, H. Yan, B. Yang, D. Liu, W. Li, H. Ade and J. Hou, A Wide Band Gap Polymer with a Deep Highest Occupied Molecular Orbital Level Enables 14.2% Efficiency in Polymer Solar Cells, *J. Am. Chem. Soc.*, 2018, **140**(23), 7159–7167.

2 L. Meng, Y. Zhang, X. Wan, C. Li, X. Zhang, Y. Wang, X. Ke, Z. Xiao, L. Ding, R. Xia, H.-L. Yip, Y. Cao and Y. Chen, Organic and Solution-Processed Tandem Solar Cells with 17.3% Efficiency, *Science*, 2018, **361**(6407), 1094–1098.

3 H. Hoppe and N. S. Sariciftci, Morphology of Polymer/Fullerene Bulk Heterojunction Solar Cells, *J. Mater. Chem.*, 2006, **16**, 45–61.

4 X. Yang and J. Loos, Toward High-Performance Polymer Solar Cells: The Importance of Morphology Control, *Macromolecules*, 2007, **40**(5), 1353–1362.

5 F. Liu, Y. Gu, J. W. Jung, W. H. Jo and T. P. Russell, On the Morphology of Polymer-Based Photovoltaics, *J. Polym. Sci., Part B: Polym. Phys.*, 2012, **50**(15), 1018–1044.

6 B. A. Collins, J. R. Tumbleston and H. Ade, Miscibility, Crystallinity, and Phase Development in P3HT/PCBM Solar Cells: Toward an Enlightened Understanding of Device Morphology and Stability, *J. Phys. Chem. Lett.*, 2011, **2**(24), 3135–3145.

7 T. M. Burke and M. D. McGehee, How High Local Charge Carrier Mobility and an Energy Cascade in a Three-Phase Bulk Heterojunction Enable >90% Quantum Efficiency, *Adv. Mater.*, 2014, **26**(12), 1923–1928.

8 S. Sweetnam, K. R. Graham, G. O. N. Ndjawa, T. Heumüller, J. A. Bartelt, T. M. Burke, W. Li, W. You, A. Amassian and M. D. McGehee, Characterization of the Polymer Energy Landscape in Polymer: Fullerene Bulk Heterojunctions with Pure and Mixed Phases, *J. Am. Chem. Soc.*, 2014, **136**(40), 14078–14088.

9 K. Jiang, G. Zhang, G. Yang, J. Zhang, Z. Li, T. Ma, H. Hu, W. Ma, H. Ade and H. Yan, Multiple Cases of Efficient Non-Fullerene Ternary Organic Solar Cells Enabled by an Effective Morphology Control Method, *Adv. Energy Mater.*, 2017, **8**(9), 1701370.

10 T. Wang, X.-K. Chen, A. Ashokan, Z. Zheng, M. K. Ravva and J.-L. Brédas, Bulk Heterojunction Solar Cells: Impact of Minor Structural Modifications to the Polymer Backbone on the Polymer–Fullerene mixing and Packing and on the Fullerene-Fullerene Connecting Network, *Adv. Funct. Mater.*, 2018, **28**(14), 1705868.

13168 | *J. Mater. Chem. C*, 2018, **6**, 13162–13170

This journal is © The Royal Society of Chemistry 2018

11 A. C. Stuart, J. R. Tumbleston, H. Zhou, W. Li, S. Liu, H. Ade and W. You, Fluorine Substituents Reduce Charge Recombination and Drive Structure and Morphology Development in Polymer Solar Cells, *J. Am. Chem. Soc.*, 2013, **135**(5), 1806–1815.

12 W. Li, S. Albrecht, L. Yang, S. Roland, J. R. Tumbleston, T. McAfee, L. Yan, M. A. Kelly, H. Ade, D. Neher and W. You, Mobility-Controlled Performance of Thick Solar Cells Based on Fluorinated Copolymers, *J. Am. Chem. Soc.*, 2014, **136**(44), 15566–15576.

13 K. Do, Q. Saleem, M. K. Ravva, F. Cruciani, Z. Kan, J. Wolf, M. R. Hansen, P. M. Beaujuge and J.-L. Brédas, Impact of Fluorine Substituents on π-Conjugated Polymer Main-Chain Conformations, Packing, and Electronic Couplings, *Adv. Mater.*, 2016, **28**(37), 8197–8205.

14 T. Wang, M. K. Ravva and J.-L. Brédas, Impact of the Nature of the Side-Chains on the Polymer–Fullerene Packing in the Mixed Regions of Bulk Heterojunction Solar Cells, *Adv. Funct. Mater.*, 2016, **26**(32), 5913–5921.

15 Z. Hu, R. T. Haws, Z. Fei, P. Boufflet, M. Heeney, P. J. Rossky and D. A. Vanden Bout, Impact of Backbone Fluorination on Nanoscale Morphology and Excitonic Coupling in Polythiophenes, *PNAS*, 2016, **114**(20), 5113–5118.

16 Z. Li, K. Jiang, G. Yang, J. Y. L. Lai, T. Ma, J. Zhao, W. Ma and H. Yan, Donor Polymer Design Enables Efficient Non-Fullerene Organic Solar Cells, *Nat. Commun.*, 2016, **7**, 13094.

17 G. Yang, Z. Li, K. Jiang, J. Zhang, J. Chen, G. Zhang, F. Huang, W. Ma and H. Yan, Optimal Extent of Fluorination Enabling Strong Temperature-Dependent Aggregation, Favorable Blend Morphology and High-Efficiency Polymer Solar Cells, *Sci. China: Chem.*, 2017, **60**(4), 545–551.

18 Z. Li, H. Lin, K. Jiang, J. Carpenter, Y. Li, Y. Liu, H. Hu, J. Zhao, W. Ma, H. Ade and H. Yan, Dramatic Performance Enhancement for Large Bandgap Thick-Film Polymer Solar Cells Introduced by a Difluorinated Donor Unit, *Nano Energy*, 2015, **15**, 607–615.

19 Y. Liu, J. Zhao, Z. Li, C. Mu, W. Ma, H. Hu, K. Jiang, H. Lin, H. Ade and H. Yan, Aggregation and Morphology Control Enables Multiple Cases of High-Efficiency Polymer Solar Cells, *Nat. Commun.*, 2014, **5**, 5293.

20 J. Zhao, Y. Li, G. Yang, K. Jiang, H. Lin, H. Ade, W. Ma and H. Yan, Efficient Organic Solar Cells Processed from Hydrocarbon Solvents, *Nat. Energy*, 2016, **1**, 15027.

21 L. Ye, H. Hu, M. Ghasemi, T. Wang, B. A. Collins, J.-H. Kim, K. Jiang, J. H. Carpenter, H. Li, Z. Li, T. McAfee, J. Zhao, X.-K. Chen, J. L. Y. Lai, T. Ma, J.-L. Brédas, H. Yan and H. Ade, Quantitative Relations between Interaction parameter, Miscibility and Function in Organic Solar Cells, *Nat. Mater.*, 2018, **17**, 253–260.

22 L. Lu, T. Zheng, Q. Wu, A. M. Schneider, D. Zhao and L. Yu, Recent Advances in Bulk Heterojunction Polymer Solar Cells, *Chem. Rev.*, 2015, **115**(23), 12666–12731.

23 C. J. Brabec, M. Heeney, I. McCulloch and J. Nelson, Influence of Blend Microstructure on Bulk Heterojunction Organic Photovoltaic Performance, *Chem. Soc. Rev.*, 2011, **40**, 1185–1199.

24 N. C. Cates, R. Gysel, Z. Beiley, C. E. Miller, M. F. Toney, M. Heeney, I. McCulloch and M. D. McGehee, Tuning the Properties of Polymer Bulk Heterojunction Solar Cells by Adjusting Fullerene Size to Control Intercalation, *Nano Lett.*, 2009, **9**(12), 4153–4157.

25 C. Piliego, T. W. Holcombe, J. D. Douglas, C. H. Woo, P. M. Beaujuge and J. M. J. Fréchet, Synthetic Control of Structural Order in *n*-alkylthieno[3,4-*c*]pyrrole-4,6-dione-Based Polymers for Efficient Solar Cells, *J. Am. Chem. Soc.*, 2010, **132**(22), 7595–7597.

26 Z. Li, S.-W. Tsang, X. Du, L. Scoles, G. Robertson, Y. Zhang, F. Toll, Y. Tao, J. Lu and J. Ding, Alternating Copolymers of cyclopenta [2,1-*b*;3,4-*b'*] dithiophene and Thieno[3,4-*c*]pyrrole-4,6-dione for High-Performance Polymer Solar Cells, *Adv. Funct. Mater.*, 2011, **21**(17), 3331–3336.

27 K. R. Graham, C. Cabanetos, J. P. Jahnke, M. N. Idso, A. E. Labban, G. O. N. Ndjawa, T. Heumueller, K. Vandewal, A. Salleo, B. F. Chmelka, A. Amassian, P. M. Beaujuge and M. D. McGehee, Importance of the Donor: Fullerene Intermolecular Arrangement for High-Efficiency Organic Photovoltaics, *J. Am. Chem. Soc.*, 2014, **136**(27), 9608–9618.

28 K. Do, M. K. Ravva, T. Wang and J.-L. Brédas, Computational Methodologies for Developing Structure–Morphology–Performance Relationships in Organic Solar Cells: A Protocol Review, *Chem. Mater.*, 2017, **29**(1), 346–354.

29 W. L. Jorgensen and J. Tirado-Rives, The OPLS [optimized potentials for liquid simulations] Potential Functions for Proteins, Energy Minimizations for Crystals of Cyclic Peptides and Crambin, *J. Am. Chem. Soc.*, 1988, **110**(6), 1657–1666.

30 D. L. Cheung and A. Troisi, Theoretical Study of the Organic Photovoltaic Electron Acceptor PCBM: Morphology, Electronic Structure, and Charge Localization, *J. Phys. Chem. C*, 2010, **114**(48), 20479–20488.

31 M. K. Dahlgren, P. Schyman, J. Tirado-Rives and W. L. Jorgensen, Characterization of Biaryl Torsional Energetics and its Treatment in OPLS All-Atom Force Fields, *J. Chem. Inf. Model.*, 2013, **53**(5), 1191–1199.

32 N. E. Jackson, K. L. Kohlstedt, B. M. Savoie, M. O. de la Cruz, G. C. Schatz, L. X. Chen and M. A. Ratner, Conformational Order in Aggregates of Conjugated Polymers, *J. Am. Chem. Soc.*, 2015, **137**(19), 6254–6262.

33 M. J. Frisch, G. W. Trucks, H. B. Schlegel, G. E. Scuseria, M. A. Robb, J. R. Cheeseman, G. Scalmani, V. Barone, B. Mennucci, G. A. Petersson, H. Nakatsuji, M. Caricato, X. Li, H. P. Hratchian, A. F. Izmaylov, J. Bloino, G. Zheng, J. L. Sonnenberg, M. Hada, M. Ehara, K. Toyota, R. Fukuda, J. Hasegawa, M. Ishida, T. Nakajima, Y. Honda, O. Kitao, H. Nakai, T. Vreven, J. A. Montgomery Jr, J. E. Peralta, F. Ogliaro, M. Bearpark, J. J. Heyd, E. Brothers, K. N. Kudin, V. N. Staroverov, R. Kobayashi, J. Normand, K. Raghavachari, A. Rendell, J. C. Burant, S. S. Iyengar, J. Tomasi, M. Cossi, N. Rega, J. M. Millam, M. Klene, J. E. Knox, J. B. Cross, V. Bakken, C. Adamo, J. Jaramillo, R. Gomperts, R. E. Stratmann, O. Yazyev, A. J. Austin, R. Cammi, C. Pomelli, J. W. Ochterski, R. L. Martin, K. Morokuma, V. G. Zakrzewski, G. A. Voth, P. Salvador, J. J. Dannenberg, S. Dapprich,

This journal is © The Royal Society of Chemistry 2018

J. Mater. Chem. C, 2018, **6**, 13162–13170 | 13169

A. D. Daniels, Ö. Farkas, J. B. Foresman, J. V. Ortiz, J. Cioslowski and D. J. Fox, *Gaussian 09, Revision D.01*, Gaussian, Inc., Wallingford, CT, 2009.

34 F.-Y. Dupradeau, A. Pigache, T. Zaffran, C. Savineau, R. Lelong, N. Grivel, D. Lelong, W. Rosanski and P. Cieplak, The REd. Tools: Advances in RESP and ESP Charge Derivation and Force Field Library Building, *Phys. Chem. Chem. Phys.*, 2010, **12**(28), 7821–7839.

35 R. A. Marcus, Electron Transfer Reactions in Chemistry. Theory and Experiment, *Rev. Mod. Phys.*, 1993, **65**, 599–610.

36 V. Coropceanu, J. Cornil, D. A. da Silva Filho, Y. Oliver, R. Silbey and J.-L. Brédas, Charge-Transport in Organic Semiconductors, *Chem. Rev.*, 2007, **107**(4), 926–952.

37 S. F. Boys and F. Bernardi, The Calculation of Small Molecular Interactions by the Differences of Separate Total Energies. Some Procedures with Reduced Errors, *Mol. Phys.*, 1970, **19**(4), 553–566.

38 C. B. Nielsen, A. J. P. White and I. McCulloch, Effects of Fluorination of 2,1,3-Benzothiadiazole, *J. Org. Chem.*, 2015, **80**(10), 5045–5048.